



HAL
open science

The origins of nearly coplanar, non-resonant systems of close-in super-Earths

Leandro Esteves, André Izidoro, Sean Raymond, Bertram Bitsch

► **To cite this version:**

Leandro Esteves, André Izidoro, Sean Raymond, Bertram Bitsch. The origins of nearly coplanar, non-resonant systems of close-in super-Earths. *Monthly Notices of the Royal Astronomical Society*, 2020, 497 (2), pp.2493-2500. 10.1093/mnras/staa2112 . hal-02997994

HAL Id: hal-02997994

<https://hal.science/hal-02997994>

Submitted on 26 Aug 2022

HAL is a multi-disciplinary open access archive for the deposit and dissemination of scientific research documents, whether they are published or not. The documents may come from teaching and research institutions in France or abroad, or from public or private research centers.

L'archive ouverte pluridisciplinaire **HAL**, est destinée au dépôt et à la diffusion de documents scientifiques de niveau recherche, publiés ou non, émanant des établissements d'enseignement et de recherche français ou étrangers, des laboratoires publics ou privés.

The origins of nearly coplanar, non-resonant systems of close-in super-Earths

Leandro Esteves¹, André Izidoro^{1,2}, Sean N. Raymond³ and Bertram Bitsch⁴

¹UNESP, Universidade Estadual Paulista, Grupo de Dinâmica Orbital e Planetologia, Guaratinguetá, CEP 12516-410, SP, Brazil

²Department of Earth, Environmental and Planetary Sciences, MS 126, Rice University, Houston, TX 77005, USA

³Laboratoire d'astrophysique de Bordeaux, Univ. Bordeaux, CNRS, B18N, allée Geoffroy Saint-Hilaire, F-33615 Pessac, France

⁴Max-Planck-Institut für Astronomie, Königstuhl 17, D-69117 Heidelberg, Germany

Accepted 2020 July 13. Received 2020 July 13; in original form 2019 December 19

ABSTRACT

Some systems of close-in ‘super-Earths’ contain five or more planets on non-resonant but compact and nearly coplanar orbits. The Kepler-11 system is an iconic representative of this class of system. It is challenging to explain their origins given that planet–disc interactions are thought to be essential to maintain such a high degree of coplanarity, yet these same interactions invariably cause planets to migrate into chains of mean motion resonances. Here, we mine a large data set of dynamical simulations of super-Earth formation by migration. These simulations match the observed period ratio distribution as long as the vast majority of planet pairs in resonance become dynamically unstable. When instabilities take place resonances are broken during a late phase of giant impacts, and typical surviving systems have planet pairs with significant mutual orbital inclinations. However, a subset of our unstable simulations matches the Kepler-11 system in terms of coplanarity, compactness, planet-multiplicity, and non-resonant state. This subset has dynamical instability phases typically much shorter than ordinary systems. Unstable systems may keep a high degree of coplanarity post-instability if planets collide at very low orbital inclinations ($\lesssim 1^\circ$) or if collisions promote efficient damping of orbital inclinations. If planetary scattering during the instability takes place at low orbital inclinations ($\lesssim 1^\circ$), orbital inclinations are barely increased by encounters before planets collide. When planetary scattering pumps orbital inclinations to higher values ($\gtrsim 1^\circ$) planets tend to collide at higher mutual orbital inclinations, but depending on the geometry of collisions mergers’ orbital inclinations may be efficiently damped. Each of these formation pathways can produce analogues to the Kepler-11 system.

Key words: planets and satellites: formation – protoplanetary discs.

1 INTRODUCTION

At least 30 per cent of main-sequence stars host planets with sizes between 1 and 4 Earth radii or masses less than $20 M_\oplus$ on orbital periods shorter than 100 d (Mayor et al. 2011; Howard et al. 2012; Winn & Fabrycky 2015). This population contains both high- and low-density planets (Rogers 2015; Wolfgang, Rogers & Ford 2016). Given that our focus is solely on their formation, we refer to this entire category of planets as *hot super-Earths*.

Two key constraints on formation models are the observed multiplicity and period ratio distributions of super-Earths. Among transiting super-Earth systems only ~ 20 per cent are found in multiple planets systems ($N > 2$). The remaining ~ 80 per cent contain only a single *transiting* planet (Fang & Margot 2012; Johansen et al. 2012; Tremaine & Dong 2012). This has been called the Kepler dichotomy, and it is not clearly found in radial velocity systems (e.g. Figueira et al. 2012). Adjacent super-Earths in multiplanet systems are rarely found in mean motion resonances (Fabrycky et al. 2014).

Notable exceptions include the Kepler-223 (Mills et al. 2016) and TRAPPIST-1 (Gillon et al. 2017; Luger et al. 2017) systems.

The migration model proposes that super-Earths formed at larger distances from their stars and migrated inwards by interactions with gaseous protoplanetary discs (Terquem & Papaloizou 2007; Ida & Lin 2010; McNeil & Nelson 2010). In this model super-Earths pile up near the disc’s inner edge, forming long chains of planets locked in first-order mean motion resonances. After the gas disc dissipates (or just before), most resonant chains become dynamically unstable (Izidoro et al. 2017, 2019). We call systems ‘unstable’ if they undergo a phase of instability near the end of the gas disc lifetime and refer to the phase of subsequent collisions as the ‘late instability phase’. Instability triggers scattering events among planets, breaks resonances and leads to giant impacts. Close to the star collisions are favoured with respect to ejections because of high escape velocities from the star and short orbital periods (e.g. Safronov 1972; Cossou et al. 2014; Izidoro et al. 2017, 2019; Raymond et al. 2018b; Izidoro et al. 2019; Lambrechts et al. 2019). Surviving systems have orbits that are more spread out and dynamically excited than in the resonant chain phase. Systems that do not go dynamically unstable and stay in long resonant chains during the entire course of the simulations from Izidoro et al. (2019) are referred as ‘stable’ systems. These simulations do not take into account other

* E-mail: leandro-esteves@hotmail.com (LE); izidoro.costa@gmail.com (AI)

potential mechanisms that may help to trigger dynamical instabilities – in systems that remained stable during the entire course of their simulations – as for instance the effects of tidal dissipation, general relativity, planetesimal scattering and magnetospheric rebound (e.g. Bolmont et al. 2014; Goldreich & Schlichting 2014; Chatterjee & Ford 2015; Liu, Ormel & Lin 2017). Here we assume that the instability phase is the source of the observed period ratio distribution of super-Earth systems.

Simulations show that the migration model matches the period ratio distribution of Kepler super-Earths if 90–99 per cent of resonant chains become unstable (Izidoro et al. 2017, 2019). The same sample of systems matches the Kepler dichotomy because the considerable mutual inclinations between planetary orbits decreases the probability of finding many planets transiting in the same system (see also Mulders et al. 2018). This argues that most single-transit systems are inherently multiple planet systems, in agreement with radial velocity surveys (e.g. Figueira et al. 2012).

At first glance the migration model predicts that all stable systems should end up with many planets on coplanar, resonant orbits. When the viewing geometry is aligned with the planets’ orbital plane, many planets should be detected in transit. In contrast, unstable systems should produce planets on non-coplanar, non-resonant orbits. Rarely should many planets be found to transit in the same system in this case.

There exists an observed category of system that is hard to understand in the framework of the migration model that contains many transiting planets on near-coplanar but non-resonant orbits. The Kepler-11 (Lissauer et al. 2011) and Kepler-20 (Fressin et al. 2012; Gautier et al. 2012) systems are representative members of this class (see Fig. 1). Six planets are known to transit in Kepler-11 with orbital periods between 10 and 118 d (semimajor axis between 0.091 and 0.466 au) and mutual orbital inclinations of at most 1° or 2° (Lissauer et al. 2013). The Kepler-20 system hosts two Earth-sized planets and four larger super-Earths, all with orbital periods between 3.69 and 77.61 d (semimajor axis between 0.045 and ~ 0.345 au). Five of the six planets transit their star, but the second-outermost planet was discovered with the radial velocity technique (Buchhave et al. 2016). Kepler-11’s and Kepler-20’s stellar ages have been estimated at 3.2 ± 0.9 Gyr (Bedell et al. 2017) and 7.6 ± 3.7 Gyr (Buchhave et al. 2016), respectively, indicating that each system is long-term stable (see also Migaszewski, Słonina & Goździewski 2012; Hands, Alexander & Dehnen 2014; Mahajan & Wu 2014; Mia & Kushvah 2016; Jontof-Hutter et al. 2017).

Our paper is laid out as follows. In Section 2, we present the set-up of our simulations. Next, we describe how we mined the outcome of these simulations to find 12 Kepler-11 analogue systems (Section 3). In Section 4, we show the typical formation pathway of these systems. We discuss our results and their implications in Section 5.

2 SIMULATIONS

We simulated the growth and dynamical evolution of systems of super-Earths during and after the gaseous disc phase (following from Izidoro et al. 2019). Our code is based on the *N*-body code *Mercury* (Chambers 1999), to which we have added synthetic forces designed to mimic essential planet formation processes. These include a prescription for disc evolution and dispersal (following Bitsch et al. 2015), growth of planetary embryos by pebble accretion (Johansen & Lambrechts 2017), adopting a simple model for how the pebble flux evolves in time (Izidoro et al. 2019), tidal interactions between growing planets and the gas disc that lead to eccentricity and inclination damping (Tanaka & Ward 2004; Cresswell & Nelson

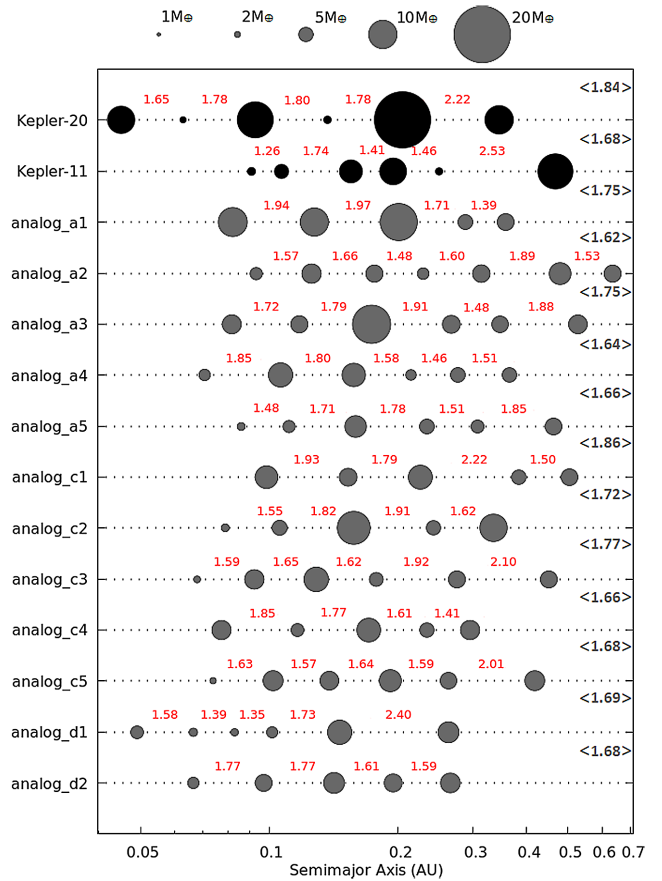


Figure 1. A selection of simulated planetary systems with dynamical architectures similar to those of Kepler-11 and Kepler-20 (shown at the top). Each horizontal line shows a full system. The planet size scales with mass. For the estimated masses of Kepler-11 and Kepler-20 planets, we follow Bedell et al. (2017) and Buchhave et al. (2016), respectively. As estimated masses are not available for Kepler-11g, Kepler-20e, and Kepler-20f we estimated their masses using the mass-radius relationship from Wolfgang et al. (2016). The red numbers between planet pairs show the period ratio of the respective planet pair. The black numbers on the far right show the mean period ratio of each system. Size of the dots scales linearly with mass as shown at the top. The planets in the figure have orbital eccentricities ranging from 0.0034 to 0.099, and the whole simulated sample mean eccentricity is 0.0292. We recall that simulations from Izidoro et al. (2019) do not take into account gas accretion on to planetary embryos.

2008) as well as orbital migration (Ward 1997; Paardekooper, Baruteau & Kley 2011). Collisions between growing bodies occur naturally and are treated as inelastic mergers, conserve mass, and linear momentum.

Our analysis is based on a subset of simulations from Izidoro et al. (2019), specifically their model I, II, and III runs. Our simulations start from a distribution of planetary seeds with masses of 0.005–0.015 Earth masses extending from either 0.7 to 20 au (model I, *a* and *b* analogue indexes), 0.7 to 60 au (model II, *c*), or 0.2 to 2 au (model III, *d*). Simulations of model I from Izidoro et al. (2019) with nominal pebble flux and disc age (model I, *b*) did not produce Kepler-11 analogues (see discussion below).

Seeds were given small but non-zero starting inclinations and eccentricities. Our simulations invoke a flux of pebbles spiralling inward through the disc due to aerodynamic drag (see e.g. Lambrechts & Johansen 2014). The inner edge of the gaseous disc was set at 0.1 au, consistent with analyses of the Kepler super-Earths (Mulders et al.

2018) and as also found from radiation hydrodynamical simulations of the inner disc edge (Flock et al. 2019). The different models make different assumptions about the pebble size in the inner rocky parts of the disc as well as the disc mass at the start of the simulation, calibrated to match a given time in the evolution of our canonical disc model (taken from Bitsch et al. 2015). In our simulations, seeds grow by accreting pebbles and eventually become massive enough to migrate (all the while continuing to accrete pebbles). Convergent migration leads to collisions among growing seeds, which feeds back on the migration rate. Growing planets may eventually reach pebble isolation mass (Bitsch et al. 2018), where the pebble isolation mass in the inner disc regions could explain the presumed masses of the Kepler planets (e.g. Bitsch 2019; Wu 2019). After the dissipation of the gaseous disc, each simulation was integrated for another 50 Myr taking only gravitational perturbations into account. Simulations from Izidoro et al. (2019) do not take into account gas accretion on to planetary embryos. For full technical details of the code and set-up, see Izidoro et al. (2019), Bitsch et al. (2019), and Lambrechts et al. (2019).

In our analysis, we made use of the subset of simulations from Izidoro et al. (2019) that formed super-Earth systems roughly consistent with observations in terms of their masses (see Wolfgang et al. 2016) and period ratio distributions (see Fabrycky et al. 2014). This amounts to a total of 221 simulations.

3 MINING OUR SIMULATIONS FOR KEPLER-11 AND KEPLER-20 ANALOGUES

Fig. 1 shows the orbital architecture of 12 Kepler-11-like systems selected from our simulations.

We used four criteria to select Kepler-11 analogues, applied to planets within 0.7 au:

- (i) Systems could not contain more than one planet pair in first-order mean motion resonance. The so-called stable systems do not match this first constraint so all our selected systems come from unstable systems of Izidoro et al. (2019).
- (ii) Systems must have mean period ratios between adjacent planets within ± 15 per cent of the Kepler-11 value of 1.68.
- (iii) Mutual inclinations between planetary orbits must be small enough that five or more planets could be observed in transit.
- (iv) Systems must maintain dynamical stability and criteria 1–3 over at least 1 billion years when we extend our simulations from 50 Myr to 1 Gyr.

We will discuss how the fraction of Kepler-11-like systems in our simulations compare to observations in Section 5.

A nice example simulation – *analog_c5* – contains six planets between 0.07 and 0.42 au. Only the outermost pair of super-Earths appears to be in 2:1 resonance (in fact one of the resonant angles associated with the 2:1 mean motion resonance librates and circulates). The mean period ratio between planets in this system is 1.688, very close to the Kepler-11 value of 1.68 (The mean period ratio of the Kepler-20 planet pairs is ~ 1.84). Considering the estimated masses of the Kepler-11 and Kepler-20 planets (Lissauer et al. 2011; Buchhave et al. 2016; Wolfgang et al. 2016; Bedell et al. 2017), we have also calculated the mean mutual Hill radii of these systems. To calculate the mean Hill radius of each system, we first calculated the mutual Hill radii of adjacent-planet pairs in the system and then we average over the pairs in the system.

Using the upper and lower limits of their estimated masses, the mean mutual hill radii of the Kepler-11 system are 12.85 and 14.45, respectively. For the Kepler-20 system, these metrics ranges between

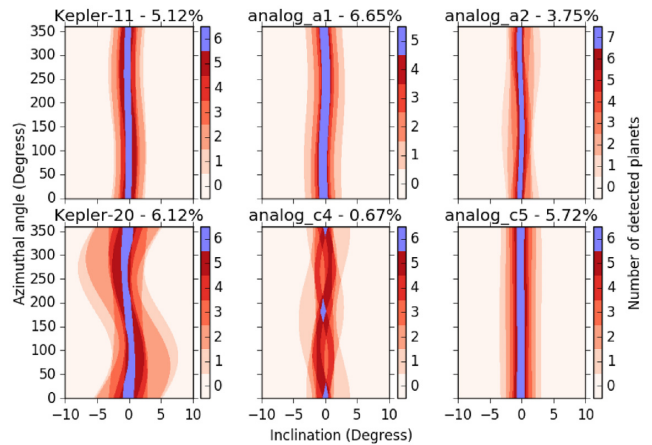


Figure 2. A geometric transit map for a model Kepler-11, Kepler-20, and four simulated systems (data from Bedell et al. 2017; Buchhave et al. 2016, respectively). The vertical axis represents the azimuthal line of sight whereas the horizontal axis is the inclination of an observer’s line of sight relative to the system’s ecliptic plane. The colour scale indicates the number of planets that transit for each observing geometry. The percentage next to each system name indicates the fraction of viewing angles from which all planets transit. Orbital inclination data for planet Kepler-20g and eccentricity of Kepler-20d are uncertain, so we assumed the values 0.2° and 1.3° , respectively, within data upper limit.

14.35 and 16.10. The mean separation in mutual Hill radii of our 12 selected systems are between 13 and 16.5. The mean mutual Hill radii of *analog_c5* is 14.76. This shows that the compactness of our selected systems compares well with those of Kepler-11 and Kepler-20 systems not only in terms of orbital period ratio of adjacent planet pairs but also in terms of their mutual Hill radius. Thus, both Kepler-11 and Kepler-20 systems are consistent as being the outcome of dynamical instabilities rather than being necessarily the outcome of type I migration in inviscid discs that may produce compact systems that fail to form resonant chains (McNally, Nelson & Paardekooper 2019).

To estimate the probability of finding multiple planet systems, we simulated the geometric transit probability from a range of observing angles. Fig. 2 shows how the detectability of five simulated systems varies as a function of the azimuthal angle ϕ_{obs} of an observer along a reference plane and the inclination of the observer i_{obs} with respect to that same plane. Each axis was divided into 200 points and at each point and for each planet in a given system, we calculated the height of the planet relative to the system reference plane z_{planet} and the height of the observer z_{obs} relative to same plane. We imposed a minimum impact parameter of 0.9 (such that $z_{\text{det}} \leq 0.9r_{\text{star}}$) to indicate a transit detection for a given planet.

The colour scale in Fig. 2 illustrates the number of planets detected in transit at each line of sight. For an almost perfectly coplanar system, the region the number of planets seen in transit is roughly independent of the azimuthal angle and varies simply with the observer’s inclination relative to the plane of the planets. That would amount to a vertical line in Fig. 2. However, in some systems (e.g. *analog_c4*) certain azimuthal angles are preferred, representing special alignments, e.g. where the longitudes of ascending node of multiple planets cross. The amplitude of inclination that each planet covers in the figure is inversely proportional to its distance from the star.

Fig. 2 shows that in many simulated systems five or more planets could be detected in transit. Of course, this only represents a snapshot

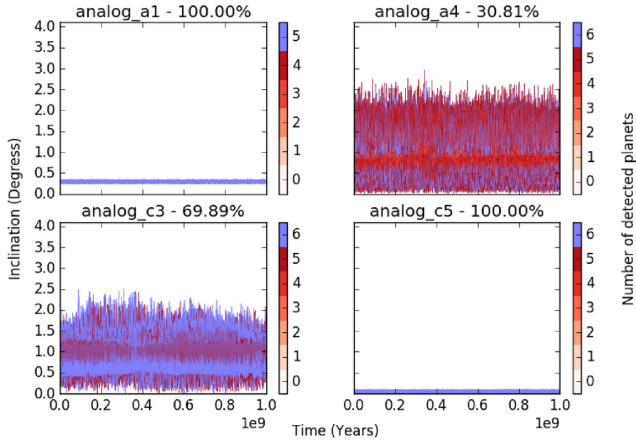


Figure 3. Long-term evolution of the planets’ orbital inclination in four different systems simulated for 1 billion years. At each time interval, the colours indicate the number of planets in transit. Each panel show the orbital inclinations of all planets in the system. Upper-left and bottom-right panels show that planets’ orbital inclinations in these systems vary over a very small range. The percentage next to the name of each system represents the fraction of the integration during which all of the planets in a given system would be found to transit.

in time. To understand the long-term evolution of these systems, and to ensure that their transit detection is maintained, we integrated these systems for 1 Gyr past their final configuration at 50 Myr obtained from Izidoro et al. (2019). We only included planets within 0.7 au to reduce the computing time need.

The systems in Fig. 1 are those that maintained dynamical stability during their long-term integrations. We have extended the simulations of Izidoro et al. (2019) using the hybrid integration algorithm of Mercury package (Chambers 1999). We use an integration time-step smaller than 1/20 of the orbital period of innermost planet in the system. Any additional instability phase would reduce the system planet multiplicity, spread out the planets’ orbits, and increase mutual inclinations, likely making it impossible to detect many planets in transit. Five of our initial candidates in fact became unstable in our long-term integrations and were discarded, and they are not shown in Fig. 1. Fig. 3 shows the evolution of the planets’ inclinations in four systems that remained stable for 1 Gyr. The colour scale represents the number of planets seen in transit for an observer at $\phi_{\text{obs}} = 0$ and $i_{\text{obs}} = 0$ over the systems evolution. Two systems (analogues a1 and c5) maintained extremely low mutual inclinations and the full 5–6 planet systems are seen in transit throughout. This may be analogous to Kepler-11 (see Fig. 2). However, in two other cases (a4 and c3) the number of planets seen in transit changes in time as the planets exchange orbital angular momentum, inducing fluctuations in mutual inclinations. This may be representative of the Kepler-20 system, in which only five of six known planets transit.

4 FORMATION PATHWAYS OF KEPLER-11 ANALOGUE SYSTEMS

We now investigate the formation of the Kepler-11 analogue systems selected in the previous section. The top panel of Fig. 4 shows the mean orbital inclination of planets just before they collide (when they touch) during the instability phase and the final mergers’ orbital inclinations. Each point/star represents the mean value calculated over all planets colliding in a given system during the instability phase. Kepler-11-like systems come in two flavours. They have

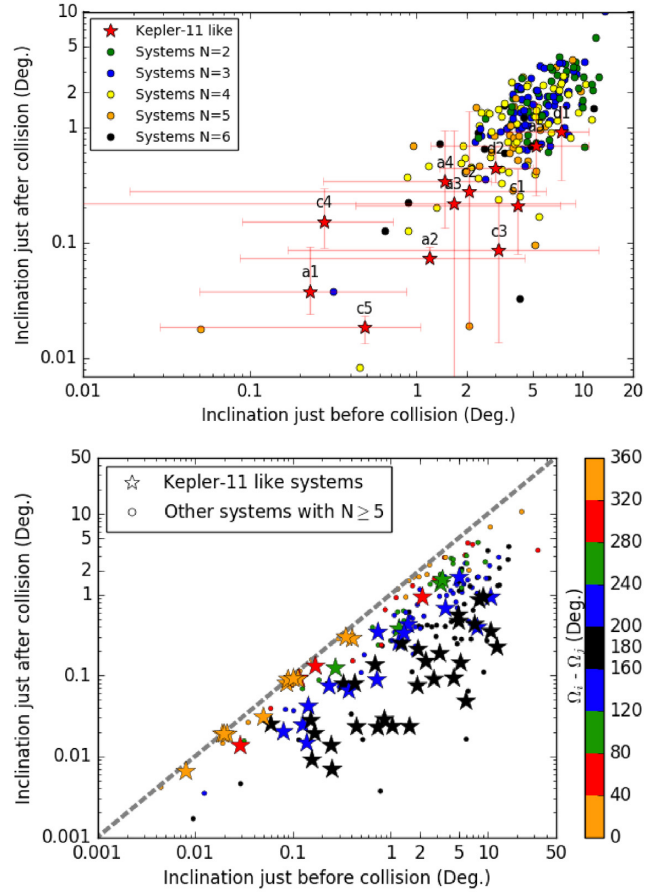


Figure 4. *Top panel:* Mean orbital inclination of planets just before collisions in the instability phase and the final mergers’ mean orbital inclinations. Each data point shows the mean values of one planetary system. The mean orbital inclination just before collision of each system is calculated averaging over all colliding planet pairs of the system but taking the maximum inclination of each planet-pair. Kepler-11-like systems are shown as red stars. Non-Kepler-11-like systems appear as dots where dot-colours represent the number of planets in the system inside 0.7 au. Inclinations are given with respect to gas disc mid-plane. The vertical and horizontal error bars show lower and upper bounds of the sample over which the respective average were calculated. Labels near the stars show the analogue name as also shown in Fig. 2. *Bottom panel:* Inclination of the merged planet as a function of the largest inclination of any two colliding bodies just before the collision. Each data point represents a single collision, unlike the top panel that shows the mean value of all collisions. Colour-coding is used to show the alignment of the longitude of the ascending node of the colliding bodies. The dashed grey line shows the identity function. Data points vertically distant from the identity function show collisions that dissipated significant inclination while those near the identity function barely affected orbital inclinations.

either very low orbital inclinations when they collide or exhibit very efficient damping of orbital inclination by collisions. Kepler-11-like systems have final planets with mean orbital inclinations typically lower than $\sim 1^\circ$. It is possible to understand these results from the lower panel of the same figure.

While the top panel of Fig. 4 show systems’ mean values, its lower panel shows the orbital inclination of individual planets (in fact this is the largest inclination of any two colliding bodies) just before they collide during the instability phase. The vertical axis show mergers inclinations just after the collisions. Again, stars show Kepler-11-like systems, but now small dots show systems with at least five planets that do not qualify as Kepler-11-like systems following our criteria.

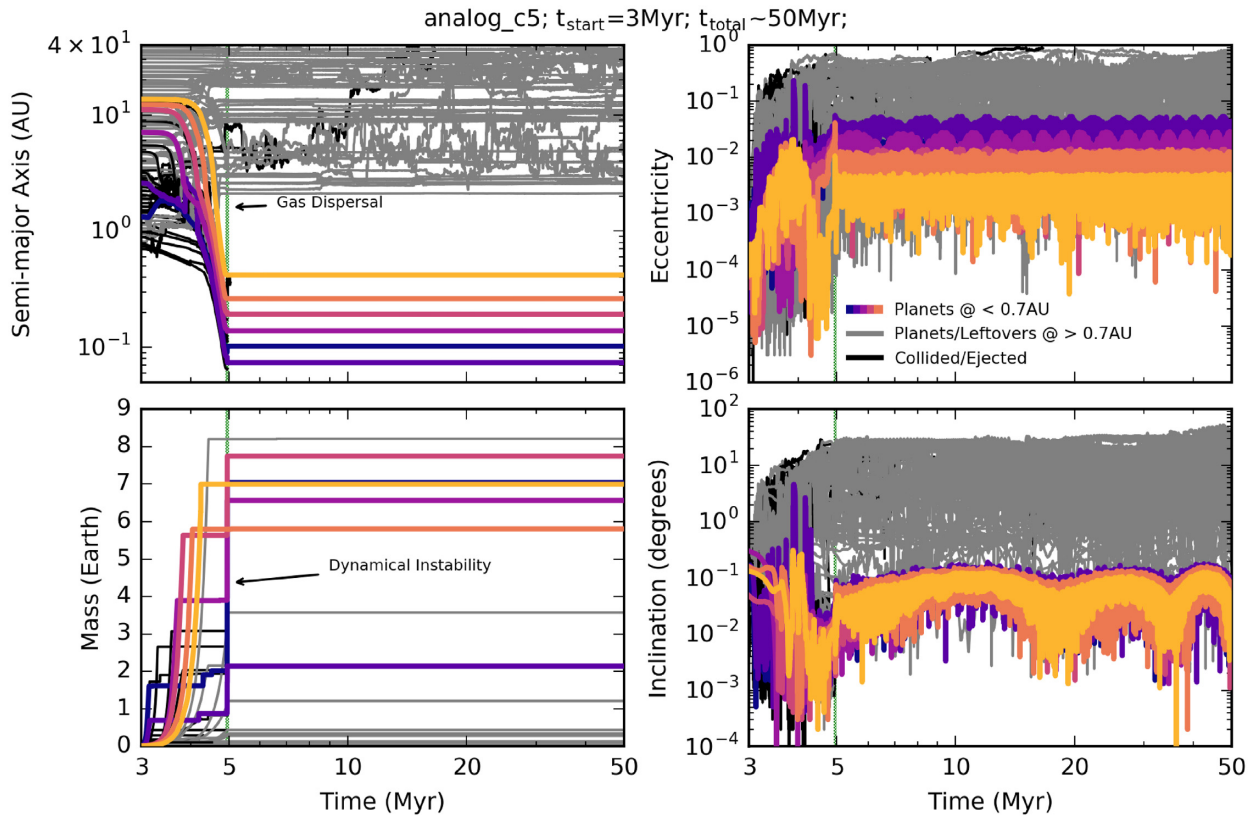


Figure 5. Formation of the *analog_c6* system. The different panels show the evolution of the growing planets’ orbital radii (top left), eccentricity (top right), mass (bottom left), and inclination (bottom right). Only planets within 0.7 au are shown in colour. More distant objects are shown in grey and those that underwent collisions in black. This simulation started at $t_{\text{start}} = 3$ Myr. The green line shows when the last phase of gas disc dissipation (from 4.9 to 5 Myr), during which a strong but short-lived instability led to a number of collisions.

The colour shows the difference of the longitude of the ascending nodes of colliding planet pairs just before the collision.

When planetary scattering during the instability phase takes place very close to the system’s invariant plane ($i < h_{\text{rmh}} = R_{\text{hill}}/a = \frac{(m_i + m_j)}{3M_{\text{star}}} \lesssim 1^\circ$; h_{rmh} is the reduced mutual Hill radius) the orbital inclination increases very slowly by encounters (Ida 1990) and planets created by mergers tend to have very low inclination orbits, independent on the bodies orbital alignment during the collision (Matsumoto & Kokubo 2017, see orange data points in the lower panel of Fig. 4). If the orbital inclination of colliding bodies is sufficiently low ($i \lesssim i_{\text{esc}} = 0.5v_{\text{esc}}/v_k$; where v_{esc} and v_k are the escape (combining the masses of i and j) and Kepler velocity, respectively) the $|v_z|$ velocity component is small and v_z is accelerated due to the gravitational focusing during the approach (Matsumoto & Kokubo 2017). If the velocity change is larger than iv_k then the longitude of the ascending nodes of the approaching bodies change such as $\Omega_i - \Omega_j \simeq 180^\circ$ and inclination gained during the encounter is mostly damped by the collision (Matsumoto & Kokubo 2017, see black data points in the lower panel of 4). If bodies eventually reach $i \gtrsim i_{\text{esc}} = 0.5v_{\text{esc}}/v_k$ during planetary scattering, gravitational focusing may not have time to align the nodes before the impact (Matsumoto & Kokubo 2017). In this case, the damping of orbital inclination may not be very efficient (e.g. red and green dots in the lower panel of Fig. 4). Damping of orbital inclination occurs in most collisions (Fig. 4) in agreement with Matsumoto & Kokubo (2017). Collisional damping of orbital inclination may occur at any distance from the star. However, because collisions are more likely to occur close to the star due to shorter dynamical time-scales and higher escape velocities

this inclination damping mechanism is probably far more efficient in close-in regions than further out.

Fig. 5 shows the growth of the planets in our best Kepler-11 analogue, the *analog_c5* system. Shortly before the final dissipation of the gas disc a dynamical instability was triggered [see for instance Goldreich & Schlichting (2014) and Pichierrri, Morbidelli & Crida (2018), Pichierrri & Morbidelli (2020) for a detailed discussion on the onset of dynamical instabilities in resonant chains]. While it led to a number of collisions, merger planets had very low (mutual) orbital inclinations because planetary scattering during the instability phase took place near the system invariant plane (in this case is also near the disc mid-plane) such that orbital inclinations grew very slowly (Ida 1990). As collisions conserve linear momentum, the merger planets also have very low mutual orbital inclinations. The instability phase in this system was quite short and ended before the gas fully dissipated. After the instability phase, there was insufficient time for planets to restore a resonant configuration before the gas fully vanished. In fact planets did not migrate significantly post-instability in this simulation. Although it is difficult to infer the exact role of the gas tidal effects for the final outcome of the dynamical instability [but see also Kominami & Ida (2002) and Iwasaki et al. (2002)] the presence of the gas disc during the stability phase is not always a required condition to produce our Kepler-11-like systems. This is the case for example for *analog_a1*. In this system, the instability phase started after the gas dispersal yet the planets remained on extremely low-inclination orbits ($\sim 0.1^\circ$). This inclination range is comparable to that of planets in *analog_c5* (Fig. 5). For the *analog_a1*, the key ingredient to produce an almost coplanar system is the fact that

planet collided at superlow mutual orbital inclinations (Matsumoto & Kokubo 2017). For systems like *analog_a1*, the eventual anti-alignment of the longitude of the ascending nodes at collisions is a mere bonus that help to damp already low orbital inclinations even further. About half of our Kepler-11 analogues underwent instabilities after the gas disc was fully gone.

The shortest instability phases of our simulated Kepler-11-like systems were for planets that collided at low orbital inclination (e.g. *analog_a4*, *analog_c5*, and *analog_a2*). We define the duration of the instability phase as the Δ_t between the timing of the first and last collision in the system. We only take into account collisions occurring later than 100 kyr before gas disc dispersal and inside 0.7 au. We expect the instability duration to depend on how fast resonances between planet pairs are broken, the orbital inclinations/eccentricities of planet pairs when this happens, and the number of planet pairs (see Pichierri et al. 2018). Unstable pairs on almost coplanar orbits collide almost immediately while inclined ones typically take longer. As the number of planets and consequently potential collisions in different unstable resonant chains may vary, we normalize the duration of the instability phase of each system (Δ_t) by the respective number of collisions during the instability phase (Δ_t/N_{col}). The quantity Δ_t/N_{col} measures the averaged time between successive collisions during the instability phase, and it is a good proxy to measure how fast collisions take place in different resonant chains. We find that in our Kepler-11-like systems the timing between successive collision is almost always shorter than 0.1 Myr (about 86 per cent of successive collisions). For a 2σ confidence level, Δ_t/N_{col} yields (0.278 ± 0.433) Myr in Kepler-11 analogues. For non-Kepler-11 analogues (with $N > 4$), it yields (2.39 ± 1.51) Myr. In Kepler-11-like systems, collisions happen fast and presumably before inclinations are significantly excited by encounters.

We also did look for other correlations that could exist between the timing of the instability phase and the dynamical state of the systems but we did not find any obvious one. This is true for instance when we measure the onset of the dynamical instability relative to the end of the gas disc dispersal (we did check this correlation for other convenient epochs). The timing of onset of the dynamical instability probably depends on the complex resonant dynamics of each resonant chain. On the other hand, the duration of the impact phase – measured via Δ_t/N_{col} – may provide insights on the dynamical state of the system when resonances are broken.

In our simulations, collisions are considered to be perfectly inelastic and conserve mass and linear momentum. To validate this assumption, we have confronted the impact data of our simulations with merging criteria for giant impacts. We find that most giant impacts during the instability phase in our simulations qualify as merging events (e.g. Kokubo & Genda 2010; Genda, Kokubo & Ida 2012; Leinhardt & Stewart 2012; Stewart & Leinhardt 2012). Fig. 6 shows the normalized impact velocities of collisions during the late instability phase with colours corresponding to merging (black) and hit-and-run (red) collisions. Only 10 per cent of collisions in our Kepler-11 systems fall in the hit-and-run regime; the other 90 per cent are merging. Thus, on average, less than one collision in Kepler-11 systems is a hit-and-run. Among our full sample of simulations the fraction of hit-and-run collisions is about 31 per cent. Our simplistic treatment of giant impacts is also supported by the results of Poon et al. (2020), who found virtually no difference between planetary systems where collisions are considered perfect merging events and where fragmentation is taken into account (see also Wallace, Tremaine & Chambers 2017). The effects of fragmentation also have minor effects on the formation of terrestrial planets in our Solar system (Chambers 2013; Clement et al. 2019).

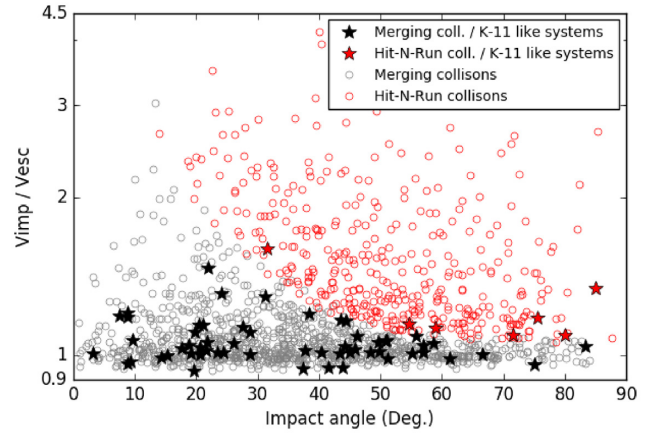


Figure 6. Normalized impact velocities for giant impacts from our simulations as a function of the impact angle. Only collisions occurring during the instability phase are shown. In addition, only those collisions where the bodies involved have masses larger than 0.6 Earth mass are shown. Collisions in Kepler-11-like systems are shown as stars and non-selected systems are shown as circles. In both cases, the black (circles or stars) show collisions that qualify as merging events and the red (circles or stars) show collisions that would qualify as hit-and-run collisions. The outcomes of our collisions are classified following the criteria by Kokubo & Genda (2010) and Genda et al. (2012).

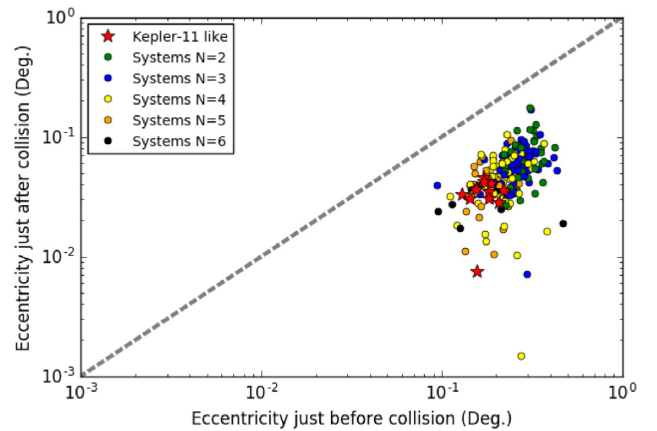


Figure 7. Mean orbital eccentricity of planets just before collisions in the instability phase and the final mergers’ mean orbital eccentricities. Each data point shows one planetary system. The mean orbital eccentricity just before collision of each system is calculated averaging over all colliding planet pairs of the system but taking the maximum eccentricity of each planet-pair. Kepler-11-like systems are shown as red stars. Non-Kepler-11-like systems appear as dots where dot-colours represent the number of planets in the system inside 0.7 au.

Finally, in Kepler-11 analogues systems the planets had also lower orbital eccentricities immediately before collisions when compared with most typical simulations, this can be seen clearly in Fig. 7. For a 2σ confidence level the mean orbital eccentricity of planet-pairs just before collisions is (0.176 ± 0.0176) for Kepler-11-like systems, while for non-Kepler-11-like systems it is (0.253 ± 0.00762) . This also supports our claim that as in Kepler-11-like systems collisions typically happen very rapidly there is virtually no time for planets to dynamically over excite each other’s orbit by mutual scattering and encounters. Fig. 7 also shows that collisions can efficiently damp orbital eccentricities which in agreement with previous studies (e.g.

Raymond, Quinn & Lunine 2006; Matsumoto, Nagasawa & Ida 2015).

5 DISCUSSION

We have shown that Kepler-11-like systems, with highly coplanar but non-resonant orbits, are a natural outcome of the migration model. Of course, they only represent a small sub-population of hot super-Earths. Yet their formation pathway – characterized by collisions at low orbital inclinations or collisions that efficiently damp orbital inclinations due to the anti-alignment of the longitude of the ascending node of colliding bodies – falls within the range of plausible outcomes of our simulations. Such systems are therefore not extreme rarities but simply modestly rare outcomes of a more general formation scenario characterized by migration of planets into resonant chains, followed by late instabilities (the so-called *breaking the chains* model; Izidoro et al. 2017, 2019).

One may wonder whether long-range migration is an essential ingredient in producing Kepler-11 analogue systems. We do not think that this is the case. Many different models have been proposed to explain the population of close-in super-Earths (see Raymond, Barnes & Mandell 2008, for a comparison between models). A common theme in all models is that super-Earths must form quickly, likely reaching near their final masses during the gaseous disc phase. This implies that the late stages of the gaseous disc phase are likely characterized by the migration of super-Earths, regardless of where and how they actually accreted (Raymond, Izidoro & Morbidelli 2018a). The *breaking the chains* model proposes that, like the awkward teenage years, resonant chains are a phase through which all super-Earth systems pass, although migration need not always imply resonant chains (McNally et al. 2019). Yet the formation of Kepler-11 analogues relies on the geometry of impacts during the instability phase.

The fraction of Kepler-11-like systems varies between different sets of simulations from Izidoro et al. (2019). Their model I – with their nominal pebble fluxes and disc ages – produced planets that were typically more than 10 Earth masses. Systems with such massive planets are typically more excited and dynamically spread and none of these systems qualified as a Kepler-11-like system considering our criteria. Kepler-11-like configurations should be more common in lower mass systems. Izidoro et al. (2019)’s model II produced five Kepler-11-like systems, with an occurrence rate of about 10 per cent of the simulations of this model. To compare our results with observations, we conducted simulated observations of our planetary systems and we find that model II systems produced 6.4 times more systems with three or more observed planets than systems with five or more planets. For the Kepler data, this same ratio is much higher, about 17. So, it is quite possible that some of our model overestimates the fraction of high multiplicity systems. However, it is important to keep in mind that high planet multiplicity systems comes in two flavours in the context of the breaking the chain scenario: from stable resonant chains such as Kepler-223 or from unstable Kepler-11-like systems. Matching the Kepler data may also require a combination of different disc models (Izidoro et al. 2019). Thus, we caution when comparing the fraction of Kepler-11-like systems produced in our simulations and those in the Kepler data.

Our simulations are admittedly simplified and we do not claim them to be the final answer in planet formation. None the less, they include a diversity of relevant physical effects thought to represent many of the key processes in planet formation. It is also reassuring that the systems we produce bear a strong resemblance to observed systems (see Izidoro et al. 2019, for a discussion).

We did not obtain systems identical to Kepler-11 and Kepler-20. Systems with very compact orbits, such as the first pair of the Kepler-11 system, almost always became unstable in our simulations. However, we note that migration can produce pairs of planets on very close orbits (Raymond et al. 2018b), which may in principle be gently separated on Gyr time-scales through tidal friction (Lithwick & Wu 2012; Batygin & Morbidelli 2013; Bolmont et al. 2014).

Looking to the future, it would be interesting to take the compositions and atmospheric envelopes of super-Earths into account together with a more sophisticated model for giant impacts, to see whether there is a correlation with coplanar non-resonant systems. It may also be important to include fragmentation in giant impact models as debris produced in the dynamical instabilities can break resonant chains if the set of debris is massive enough (Chatterjee & Ford 2015). Many planets in the Kepler-11 and Kepler-20 systems have low densities (Lissauer et al. 2013) although Kepler-20b may have a terrestrial composition (Fressin et al. 2012; Gautier et al. 2012).

ACKNOWLEDGEMENTS

We thank the referee, Ramon Brasser, for his very constructive comments and suggestions that help us to improve the paper. Leandro Esteves and André Izidoro are grateful to FAPESP for financial support through grants 17/09963-7 and 19/02936-0 (Leandro Esteves), 16/12686-2 and 16/19556-7 (André Izidoro). Bertran Bitsch thanks the European Research Council (ERC Starting Grant 757448-PAMDORA) for their financial support. André Izidoro acknowledges NASA grant 80NSSC18K0828 to Rajdeep Dasgupta, during the revision and resubmission of the work.

DATA AVAILABILITY

The data underlying this article will be shared on reasonable request to the corresponding author.

REFERENCES

- Batygin K., Morbidelli A., 2013, *AJ*, 145, 1
 Bedell M. et al., 2017, *ApJ*, 839, 94
 Bitsch B., 2019, *A&A*, 630, A51
 Bitsch B., Johansen A., Lambrechts M., Morbidelli A., 2015, *A&A*, 575, A28
 Bitsch B., Morbidelli A., Johansen A., Lega E., Lambrechts M., Crida A., 2018, *A&A*, 612, A30
 Bitsch B., Izidoro A., Johansen A., Raymond S. N., Morbidelli A., Lambrechts M., Jacobson S. A., 2019, *A&A*, 623, A88
 Bolmont E., Raymond S. N., von Paris P., Selsis F., Hersant F., Quintana E. V., Barclay T., 2014, *ApJ*, 793, 3
 Buchhave L. A. et al., 2016, *AJ*, 152, 160
 Chambers J. E., 1999, *MNRAS*, 304, 793
 Chambers J. E., 2013, *Icarus*, 224, 43
 Chatterjee S., Ford E. B., 2015, *ApJ*, 803, 33
 Clement M. S., Kaib N. A., Raymond S. N., Chambers J. E., Walsh K. J., 2019, *Icarus*, 321, 778
 Cossou C., Raymond S. N., Hersant F., Pierens A., 2014, *A&A*, 569, A56
 Cresswell P., Nelson R. P., 2008, *A&A*, 482, 677
 Fabrycky D. C. et al., 2014, *ApJ*, 790, 146
 Fang J., Margot J.-L., 2012, *ApJ*, 761, 92
 Figueira P. et al., 2012, *A&A*, 541, A139
 Flock M., Turner N. J., Mulders G. D., Hasegawa Y., Nelson R. P., Bitsch B., 2019, *A&A*, 630, A147
 Fressin F. et al., 2012, *Nature*, 482, 195
 Gautier, Thomas N. I. et al., 2012, *ApJ*, 749, 15
 Genda H., Kokubo E., Ida S., 2012, *ApJ*, 744, 137
 Gillon M. et al., 2017, *Nature*, 542, 456
 Goldreich P., Schlichting H. E., 2014, *AJ*, 147, 32

- Hands T. O., Alexander R. D., Dehnen W., 2014, *MNRAS*, 445, 749
 Howard A. W. et al., 2012, *ApJS*, 201, 15
 Ida S., 1990, *Icarus*, 88, 129
 Ida S., Lin D. N. C., 2010, *ApJ*, 719, 810
 Iwasaki K., Emori H., Nakazawa K., Tanaka H., 2002, *PASJ*, 54, 471
 Izidoro A., Ogihara M., Raymond S. N., Morbidelli A., Pierens A., Bitsch B., Cossou C., Hersant F., 2017, *MNRAS*, 470, 1750
 Izidoro A., Bitsch B., Raymond S. N., Johansen A., Morbidelli A., Lambrechts M., Jacobson S. A., 2019, preprint (arXiv:1902.08772)
 Johansen A., Lambrechts M., 2017, *Annu. Rev. Earth Planet. Sci.*, 45, 359
 Johansen A., Davies M. B., Church R. P., Holmelin V., 2012, *ApJ*, 758, 39
 Jontof-Hutter D., Weaver B. P., Ford E. B., Lissauer J. J., Fabrycky D. C., 2017, *AJ*, 153, 227
 Kokubo E., Genda H., 2010, *ApJ*, 714, L21
 Kominami J., Ida S., 2002, *Icarus*, 157, 43
 Lambrechts M., Johansen A., 2014, *A&A*, 572, A107
 Lambrechts M., Morbidelli A., Jacobson S. A., Johansen A., Bitsch B., Izidoro A., Raymond S. N., 2019, *A&A*, 627, A83
 Leinhardt Z. M., Stewart S. T., 2012, *ApJ*, 745, 79
 Lissauer J. J. et al., 2011, *Nature*, 470, 53
 Lissauer J. J. et al., 2013, *ApJ*, 770, 131
 Lithwick Y., Wu Y., 2012, *ApJ*, 756, L11
 Liu B., Ormel C. W., Lin D. N. C., 2017, *A&A*, 601, A15
 Luger R. et al., 2017, *Nat. Astron.*, 1, 0129
 Mahajan N., Wu Y., 2014, *ApJ*, 795, 32
 Matsumoto Y., Kokubo E., 2017, *AJ*, 154, 27
 Matsumoto Y., Nagasawa M., Ida S., 2015, *ApJ*, 810, 106
 Mayor M. et al., 2011, preprint (arXiv:1109.2497)
 McNeil D. S., Nelson R. P., 2010, *MNRAS*, 401, 1691
 McNally C. P., Nelson R. P., Paardekooper S.-J., 2019, *MNRAS*, 489, L17
 Mia R., Kushvah B. S., 2016, *MNRAS*, 457, 1089
 Migaszewski C., Slonina M., Goździewski K., 2012, *MNRAS*, 427, 770
 Mills S. M., Fabrycky D. C., Migaszewski C., Ford E. B., Petigura E., Isaacson H., 2016, *Nature*, 533, 509
 Mulders G. D., Pascucci I., Apai D., Ciesla F. J., 2018, *AJ*, 156, 24
 Paardekooper S. J., Baruteau C., Kley W., 2011, *MNRAS*, 410, 293
 Pichierri G., Morbidelli A., 2020, *MNRAS*, 494, 4950
 Pichierri G., Morbidelli A., Crida A., 2018, *Celest. Mech. Dyn. Astron.*, 130, 54
 Poon S. T. S., Nelson R. P., Jacobson S. A., Morbidelli A., 2020, *MNRAS*, 491, 26
 Raymond S. N., Quinn T., Lunine J. I., 2006, *Icarus*, 183, 265
 Raymond S. N., Barnes R., Mandell A. M., 2008, *MNRAS*, 384, 663
 Raymond S. N., Izidoro A., Morbidelli A., 2018a, preprint (arXiv:1812.01033)
 Raymond S. N., Boulet T., Izidoro A., Esteves L., Bitsch B., 2018b, *MNRAS*, 479, L81
 Rogers L. A., 2015, *ApJ*, 801, 41
 Safronov V. S., 1972, *IAUS*, 45, 329
 Stewart S. T., Leinhardt Z. M., 2012, *ApJ*, 751, 32
 Tanaka H., Ward W. R., 2004, *ApJ*, 602, 388
 Terquem C., Papaloizou J. C. B., 2007, *ApJ*, 654, 1110
 Tremaine S., Dong S., 2012, *AJ*, 143, 94
 Wallace J., Tremaine S., Chambers J., 2017, *AJ*, 154, 175
 Ward W. R., 1997, *Icarus*, 126, 261
 Winn J. N., Fabrycky D. C., 2015, *ARA&A*, 53, 409
 Wolfgang A., Rogers L. A., Ford E. B., 2016, *ApJ*, 825, 19
 Wu Y., 2019, *ApJ*, 874, 91

APPENDIX A: SECULAR RESONANCES IN OUR SYSTEMS

In order to further understand the dynamics of our planetary systems, we have also mined our data looking for main secular resonances in

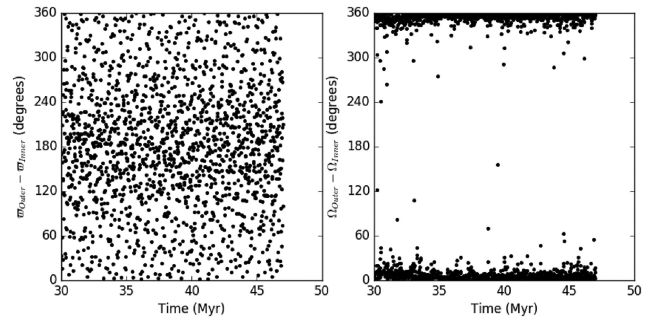


Figure A1. Time evolution of the resonance angle associated with the eccentricity-type main secular resonance (left-hand panel). As shown this angle is circulating. On the other hand, the right-hand panel shows that the resonant angle associated with the inclination-type main secular resonance is mostly librating around 0° , so this planet-pair is near/in an inclination-type secular resonance. These angles are computed considering the second and third innermost planets in the *analog_a1* system.

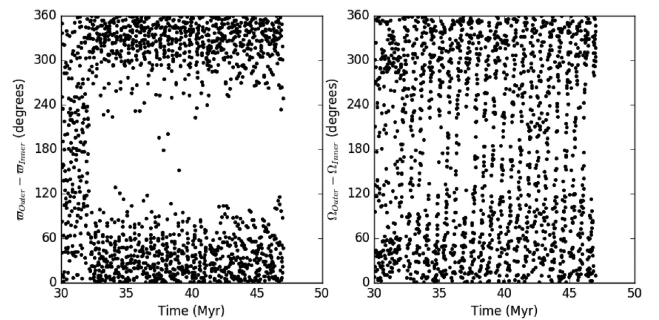


Figure A2. Same panels as in Fig. A1. Here the resonant angle associated with the eccentricity-type main secular resonance shows episodes of libration with large amplitude around 0° , while the resonant angle associated with the inclination-type main secular resonance mostly circulates. These resonant angles have been computed considering the two outermost planets of the *analog_c3* system.

our final planetary systems. From simulated planet-pairs in Fig. 1, seven planet-pairs exhibit significant (and in most cases multiple) episodes of libration of the resonance angle associated with the main inclination-type secular resonance, while the resonant angles associated with the main eccentricity-type secular resonance mostly circulate (Fig. A1). Additionally, we found another five planet-pairs where the resonant angle associated with the main secular eccentricity-type resonance showed significant (and in most cases multiple) episodes of libration, while the resonant angles associated with the main inclination-type secular resonance mostly circulated (e.g. Fig. A2, left-hand panel). Only one of our planet-pairs show episodes of libration of both angles associated with the eccentricity and inclination types main secular resonances. We consider significant episodes of libration those that last at least 1–10 Myr.

This paper has been typeset from a $\text{\TeX}/\text{\LaTeX}$ file prepared by the author.